Energy Conversion and Management 266 (2022) 115793

Contents lists available at ScienceDirect

Energy Conversion and Management

journal homepage: www.elsevier.com/locate/enconman

Development of a digital twin for real-time simulation of a combustion engine-based power plant with battery storage and grid coupling

Emma Söderäng *, Saana Hautala, Maciej Mikulski, Xiaoguo Storm, Seppo Niemi

University of Vaasa, School of Technology and Innovation, Wolffintie 34, FI-65200 Vaasa, Finland

ARTICLE INFO

Keywords:
Mid-speed engine
Squirrel cage induction generator
Battery storage
Fast-running model
Digital twin
Model-based control

ABSTRACT

Coordinated control of combustion engine-based power plants with battery storage is the next big thing for optimising renewable energy. Digital twins can enable such sophisticated control but currently are too simplistic for the required insight. This study explores the feasibility of a fully physics-based combustion engine model in real-time co-simulation with an electrical power plant model, including battery storage. A detailed, crank-angle resolved, one-dimensional model of a large-bore stationary engine is reduced to a fast-running model (FRM). This engine digital twin is coupled with a complete power plant control model, developed in Simulink. Real-time functions are tested on a dedicated rapid-prototyping system using a target computer. Measurement data from the corresponding power plant infrastructure provide validation for the digital twin. The model-in-the-loop simulations show real-time results from both the standalone combustion and electric submodels mostly within 5% of measured values. The model coupling for fully predictive simulation was tested on a desktop computer, showing expected functionality and validity within 4% and 8% of the respective measured generator and converter outputs. However, execution time of the FRM needs reducing when moving to final hardware-in-the-loop implementation of a complete power plant model.

1. Introduction

First the Kyoto Protocol of 1997 and then the 2015 Paris Agreement set formal targets and commitments for reducing greenhouse gas (GHG) emissions [1,2]. These global agreements are supported and reinforced by various local initiatives. The European Unioń s (EU) 2019 Green Deal aims to turn the political commitment into a legal obligation and a trigger for investment in all sectors of the economy [3]. In the energy generation sector, for example, the EU Emission Trading System (EU ETS) is only one of many initiatives to limit emissions and support achievement of climate neutrality by 2050 [4]. These incentives serve to boost the share of renewables (wind, hydro and solar) in overall energy generation. However, a move to these forms of renewable energy also underscores the role of distributed combustion engine-based power-generation plants, able to support and supplement the renewable sources. In 2020 the EU market for gas and liquid power plants was estimated at 30 GW volume, generating over 1 billion EUR annual turnover [5]. In turn, these power plants foster demand for low-carbon fuels.

The combustion engine supports next-generation renewable energy systems through its fast-response capability to provide on-demand power to supplement weather-dependent wind or solar energy. Combustion engine plants can go from shut-off to full load within minutes: if they have complementary battery storage, this response time to react to grid power fluctuations is cut to a matter of seconds. However, the limited energy capacity of batteries cannot support continuous demand [6]. In that sense, a hybrid engine-battery-electric plant is considered a step along the evolution path of energy generation for stationary power.

In the marine sector, the International Maritime Organization (IMO) introduced the Energy Efficiency Design Index (EEDI) to drive incremental efficiency improvement of ships [7]. It accepts that the combustion engine is expected to remain the prime mover because it satisfies the ultra-high energy density demand of long- haul shipping. As in the stationary power sector, marine propulsion hybridisation with battery-electric drive offers peak-shaving energy savings and the capability to minimise emissions while manoeuvring in harbour areas [6].

In terms of scale (order of megawatts output power), solutions for the two sectors will share the majority of their components, making it logical to combine developments in hybrid power plants for both marine and stationary applications in this review. Furthermore, although both sectors have different constraints in terms of their operating modes, emission limits and system packaging, on the cumulative level these

* Corresponding author.
E-mail address: Emma.Soderang@uwasa.fi (E. Söderäng).

https://doi.org/10.1016/j.enconman.2022.115793
Received 16 November 2021; Received in revised form 9 May 2022; Accepted 19 May 2022
Available online 26 May 2022

Nomenclature

BESS	battery energy storage system
BMEP	brake mean effective pressure
BMS	battery management system
CA	crank angle
CA50	crank angle at 50% fuel mass fraction burned
dq	direct-quadrature
DTC	direct torque control
ECMS	equivalent consumption minimisation strategy
EEDI	Energy Efficiency Design Index
ESS	energy storage system
EU	European Union
EU ETS	EU Emission Trading System
FC	frequency converter
FOC	field-oriented control
FPGA	field-programmable gate array
FRM	fast-running model
GHG	greenhouse gas
HiL	hardware-in-the-loop
IGBT	insulated-gate bipolar transistor
IMO	International Maritime Organization
PI	proportional-integral controller
PLC	programmable logic controller
PLL	phase-locked loop
PMU	power monitoring unit
RCCI	reactivity controlled compression ignition
RMS	root mean square
SCIG	squirrel cage induction generator
SoC	state of charge
SOI	start of injection
SPS	Specialized Power Systems
TET	task execution time
VEBIC	Vaasa Energy Business Innovation Centre
$I_{DC,grid}$	grid DC current [A]
$I_{DC,stator}$	stator DC current [A]
I_{BESS}	battery current [A]
V_{DC}	DC-link voltage [V]
V_0	Nominal DC-link voltage [V]
$C_{DC\text{-}link}$	Nominal DC-link capacitance [F]
SoC	Battery state of charge [%]
Q	maximum battery capacity [Ah]
$BMEP$	brake mean effective pressure [bar]
p_{max}	max. cylinder pressure [bar]
T_{exh}	exhaust temperature turbine inlet [K]
P_{gen}	generator output active power [kW]
I_{gen}	generator RMS current [A]
$\cos(\varphi)_{gen}$	generator power factor [-]
P_{fc}	FC output active power [kW]
I_{fc}	FC RMS current [A]
$\cos(\varphi)_{fc}$	FC power factor [-]

constraints are equal challenging for the power systems. They must evolve to become increasingly complex in terms of both hardware and control [8,9].

Evolution for combustion engines in both sectors drives new hardware functionalities, including variable valve actuation supporting better thermal management of advanced exhaust aftertreatment systems [10], sequential turbocharging [11] and high-pressure direct injection of both liquid and gaseous fuels [12]. This new hardware requires more sophisticated control systems, featuring closed-loop, cycle-to-cycle combustion control [13]. More radical developments include new fuels and cutting-edge, low-temperature combustion technologies like reactivity controlled compression ignition (RCCI) [14].

Turning to the electrical side of hybrid propulsion and energy generation systems, the keyword for its evolution is integration. According to Jaurola et al. [15], the propulsion and auxiliary loads are becoming integrated in marine applications, rendering new, more efficient solutions for power electronic converters. The integrated combustion-electric drive concept could provide several benefits, such as achieving optimal prime- mover loading conditions. Geertsma et al. [16] identified similar trends and particularly recognised how ship performance can be improved by complex control strategies, such as rule-based heuristic techniques, equivalent consumption minimisation strategy (ECMS) and power management through load prediction. Moreover, Ghimire et al. [17] acknowledged how developments in power electronics have enabled ship electrification. Skjong et al. [8] discussed challenges with vessel electrical power systems and identified similarities with modern power grids: vessel electrical systems are comparable to land-based standalone microgrids and hence are subjected to many of the same issues. For instance, as power system complexity increases, on-board monitoring and automated diagnostic features become essential to maximise reliability.

In short, system integration is becoming increasingly necessary for complete, predictive powertrain control. The complexity at both component and system-level, along with a demand for more rapid development, push simulation to the forefront of contemporary powertrain research. So-called digital twins - physics-based, real-time representations of the physical system - are predicted to play a more prominent role in improving the overall efficiency of hybrid powertrains.

Some of the key marine applications of digital twins are the design of energy-optimised control systems, sophisticated route planning and selection of the optimal operation strategies for hybrid vessels [18]. In their recent work, Perabo et al. [19] presented a digital twin for co-simulation of a shiṕs AC power and propulsion systems. The dynamics of the diesel engine were given by a simple transfer function. Recently, Bondarenko and Fukada [20] took a step further, proposing a more physics-based approach for a ship's digital twin. The scope of the model was limited to the relatively simple application of a two-stroke diesel engine with direct drive. The engine modelling combined the continuous time-domain mean-value engine model with the crank-angle resolved phenomenological combustion model, based on the Wiebe function. The real-time execution requirement was satisfied by transforming the combustion model to an integral form, yielding a set of nonlinear algebraic equations.

Typical applications of digital twins in power generation are in the design of complex energy management systems that strive to optimise operation to minimise both cost and emissions [21,22]. Furthermore, He et al. [23] regarded the digital twin concept as a key technology for realising smart grid solutions. The studýs authors reviewed different frameworks and potential applications for digital twins of power systems in general. The work, however, focuses on power flow applications and assumes prime-mover models to be on a very high level as black-box models. Similarly, Park et al. [22] anticipated that digital twin technology could facilitate implementation of intelligent energy management systems. They proposed using a digital twin for optimal operation scheduling for an energy storage system (ESS) in a microgrid. The combustion engine side was not taken into account in model configuration.

As evident from the above, digital twins of large-scale marine and stationary hybrid power plants are already being developed and used. One general observation on the state of the art is that most of these approaches either omit the combustion engine element or represent it in

a highly simplified manner, such as a grey/black-box model. This satisfies the real-time demand in system-level simulation but deviates from the principle of a digital twin being physics-based. This aberration is an attempt to overcome the huge phenomenological complexity of the combustion element, yet in practice renders the whole digital-twin non-transferable and non-predictive in terms of changes to combustion engine architecture or controls. The lack of complete hybrid power plant digital twins incorporating a physics-based engine element hinders co-optimisation endeavours and coordinated vessel/grid-level control strategies. This shortcoming is becoming increasingly important, as state-of-the-art combustion engines have highly nonlinear dynamics and tend to gradually adopt advanced model-based control strategies, leading to a self-learning architecture, adaptable to application and constraints [24]. Additionally, coordinated hybrid engine and battery storage power plant control is essential for reaching superior efficiency levels and for handling the increasing generation flexibility demands for grid applications.

The present work aims to fill this methodological knowledge gap regarding combustion engine-based power plants and their digital twins. A detailed, crank-angle resolved, one-dimensional model of a dedicated large-bore marine/stationary engine is reduced to a fast-running model (FRM). The iterative reduction process enables us to find the tailored balance between the real-time execution time without sacrificing the governing physics. As a highlight, the approach enables to predict the engine response to all control parameters (combustion onset; cooling water temperature, waste-gate valve setpoints etc.) and captures performance variations in ambient and fuelling conditions (pressure, temperature, humidity, fuel heating value), within the individual engine cycle. Such a fully physical engine digital twin is further coupled with a complete power-plant control model framework, developed by the authors in Simulink software using Simscape Electrical Specialized Power Systems (SPS) components. Importantly, foreseeing the future demands of energy management the implementation includes a battery storage system. The real-time coupling is tested on a dedicated rapid prototyping system based on the Speedgoat target machine. The whole framework is carefully validated against dedicated measurement data from the corresponding actual power plant infrastructure. This digital twin concept with its extended predictive capabilities on the engine side outlooks significant advantages compared to the black-box engine approaches incorporated earlier, ultimately enabling self-optimizing integrated and coordinated grid-power plant control.

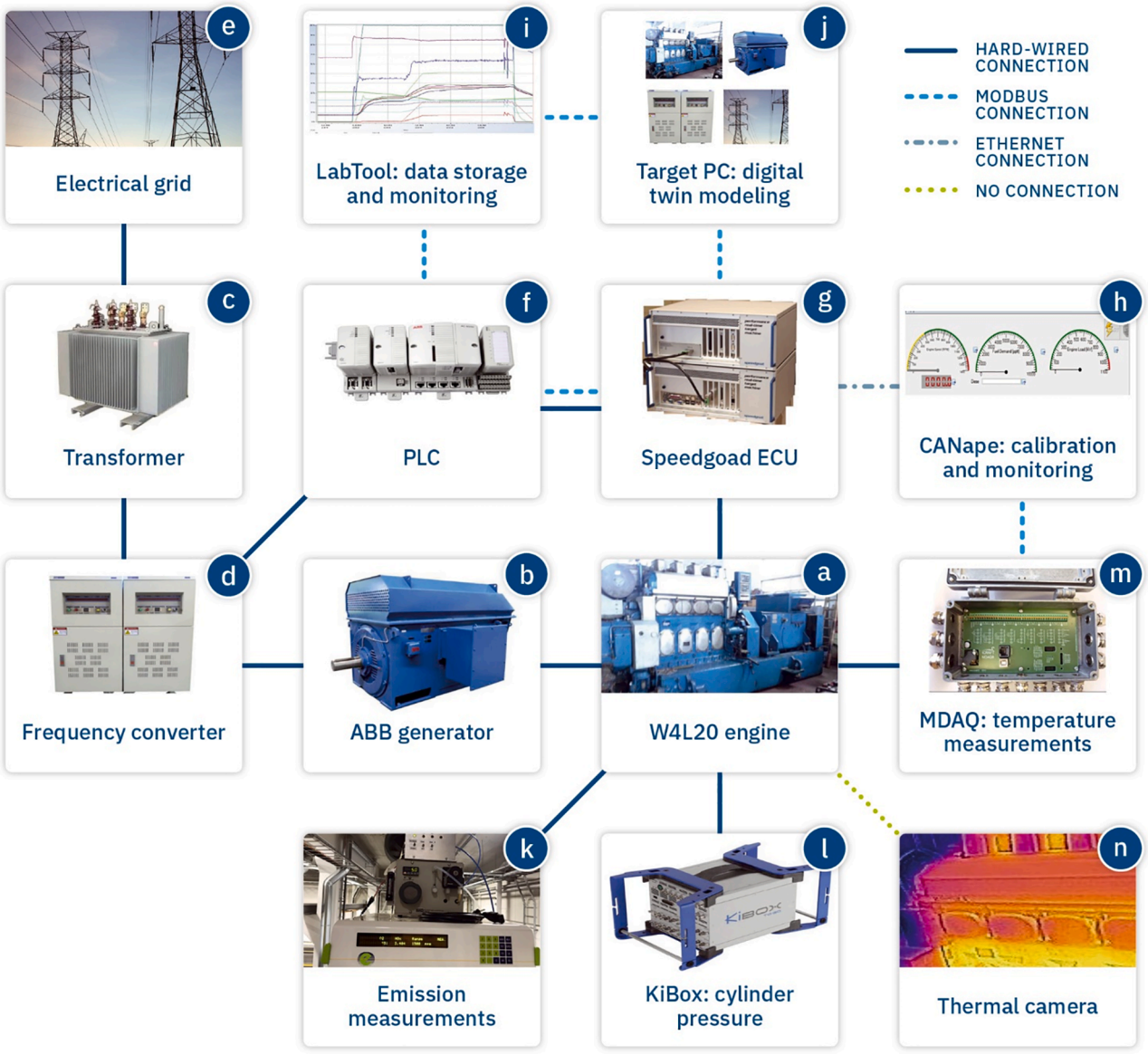

Fig. 1. VEBIC system setup including relevant measurement equipment and communication interfaces.

2. Methods

2.1. The object

The current work takes the power plant system of the Vaasa Energy Business Innovation Centre (VEBIC) as a reference for building the model. Consequently, the measurement results obtained in this facility serve for model validation. The key system components are presented schematically in Fig. 1. The complete system subjected to digitalisation incorporates a Wärtsilä 4L20 mid-speed combustion engine (Fig. 1a) coupled with an AC generator by ABB (Fig. 1b). Supplementary material A depicts the laboratory setup. The frequency converter (FC) (Fig. 1d) allows the genset to run at variable speed. Together with the 690 V/20 kV transformer (Fig. 1c), they facilitate the connection to the main AC grid (Fig. 1e). Supplementary material B illustrates the power flow by providing a simplified single-line diagram of the laboratory setup.

The following subsections detail the components most relevant to the current research, the engine and electrical interface. At this point, it is important to note that the complete system accommodates various control and data acquisition layers gathering information from both industrial (standard to the power plant installation) and research-grade measurement systems. The latter enables subsequent detailed validation of the model. The ABB programmable logic controller (PLC) is in a master row for controlling and communication in the system (Fig. 1f). As such, it is responsible for aligning the operation of the engine (Fig. 1a) and generator/FC (Fig. 1b/d) at a given load demand level. The engine control unit in this platform is implemented on Speedgoat real-time target machine (Fig. 1g) with a vast range of input–output connectivity industrial protocols. This research-grade rapid prototyping is responsible for combustion control, regulating injection parameters to achieve the optimal efficiency/emission trade-off at the given operating point. Finally, the Speedgoat communicates with other dedicated target platforms including the PC (Fig. 1j), where a digital twin of the whole system is installed.

Ultimately, the governing PLC and the Speedgoat send the electrical system-specific and engine-specific monitoring signals (Fig. 1 k/l/m) to the common data acquisition system (Fig. 1i) via a modbus interface. Slow-changing engine signals (temperatures, pressures, fuel consumption and emissions) are sampled at one-second intervals. In-cylinder pressure and injection currents are monitored by high-frequency data sampling, triggered via an optical encoder to correlate with the engine rotational angle, with 0.1 crank angle (CA) degree resolution. Relays are sampling signals related to the electrical system.

2.1.1. The Wärtsilä 4L20 engine

The whole setup depicted in Fig. 1 is powered by a Wärtsilä 4L20 mid-speed diesel engine. From the perspective of the present study, it suffices to say that this is a research version of a 200 mm-bore engine used widely in gen-set units for marine and stationary applications. The basic platform is well described in the Wärtsilä 20 Product Guide [25]. This unit is the four-cylinder version, so is more conservative on fuel consumption in laboratory conditions. It was modified for research purposes: changes include a state-of-the-art common-rail fuel injection system and a turbocharger (ABB TPS48E01) providing flexible calibration and control features. The fuel used was EN ISO 590 standard, sulphur-free diesel. The full load for the engine is 848 kW, providing 800 kW on the generator. Table 1 lists the enginés key data. Further details about the engine and its preparatory measurement systems which provided data for model calibration and validation are given in a dedicated publication by Hautala et al. [26].

2.1.2. The key electrical components

The generator in VEBIC is an ABB squirrel cage induction machine of the type M3LG 450LC 6G, with a rated output power of 1050 kW. Note, that commonly power generation systems use synchronous generators. The VEBIC laboratory, however, aside from power plant application explored in this work, serves as a dynamic engine test cell for marine and heavy mobile machinery. These applications require the ability to run highly-dynamic transient test cycles with “negative load” (for instant down-hill driving in mobile machinery with direct drive). Thus, the demand to act both as a generator and a motor with fast transients favour an induction machine over a synchronous one.

Table 1
Specification of the Wärtsilä 4L20 research engine.

Cylinder configuration	Four, inline
Bore	200 mm
Stroke	280 mm
Swept volume/cylinder	8.8 dm^3
Compression ratio	16:1
Rated speed	1000 rpm
Brake power	848 kW
Fuel system	common rail
Turbocharger	ABB TPS48E01
Valve system	four valves/cylinder, Miller timing-capable

Table 2 provides the complete specification of the generator, together with the most relevant characteristics of the accompanying power electronics. The AC generator output is handled by a 690 V, 2000 kW FC also supplied by ABB (type ACS800-17LC). This voltage source converter consists of four force-commutated, insulated-gate bipolar transistor (IGBT) inverters and four force-commutated IGBT rectifiers. They are connected back-to-back with a common DC-link, which also includes DC-link capacitors. The converter comprises a generator-side converter control system and a grid-side converter control system. In addition, there are several filters on the grid side to reduce harmonics.

A Vamp 260 power monitoring unit (PMU) and an ABB REG615 generator protection relay were used to measure root mean square (RMS) currents, active power outputs and power factors. The REG615 relay is located after the generator and the Vamp 260 is after the FC, before the transformer. The supplementary material C lists the physical system parameters used to identify and validate the electrical equipment model.

2.2. The model framework

The complete power plant model has been implemented in the Simulink environment. Fig. 2 illustrates the main subsystems and their high-level, input–output structure.

The engine model (green block in Fig. 2) is implemented as an S-function generated from third-party, one-dimensional simulation software GT-Suite, an industry standard for combustion engine simulation. As the focus of this study is to check whether the physics in the engine’s

Table 2
Generator rated data and most important parameters from the perspective of model identification.

Object/model	Parameter	Value
Generator M3LG 450LC 6G	rated power/speed	1050 kW/1007 rpm
	nominal apparent power	1200 kVA
	rated voltage	690 V ± 5%
	rated frequency	50 Hz
	rated current	1042 A
	rated power factor cos(φ)	0.87
	rated torque	−10228 Nm
	rotor/stator resistance ratio, running	0.98
	rotor/stator inductance ratio, running	0.71
	rotor inertia	39.5 kgm^2
	number of pole pairs	3
	efficiency @100% load	97.3%
Freq. converter ACS800-17LC	nominal power	2000 kW
	nominal voltage	690 V
	nominal max current for continuous loading	2035 A
	total losses @100% load	79.5 kW

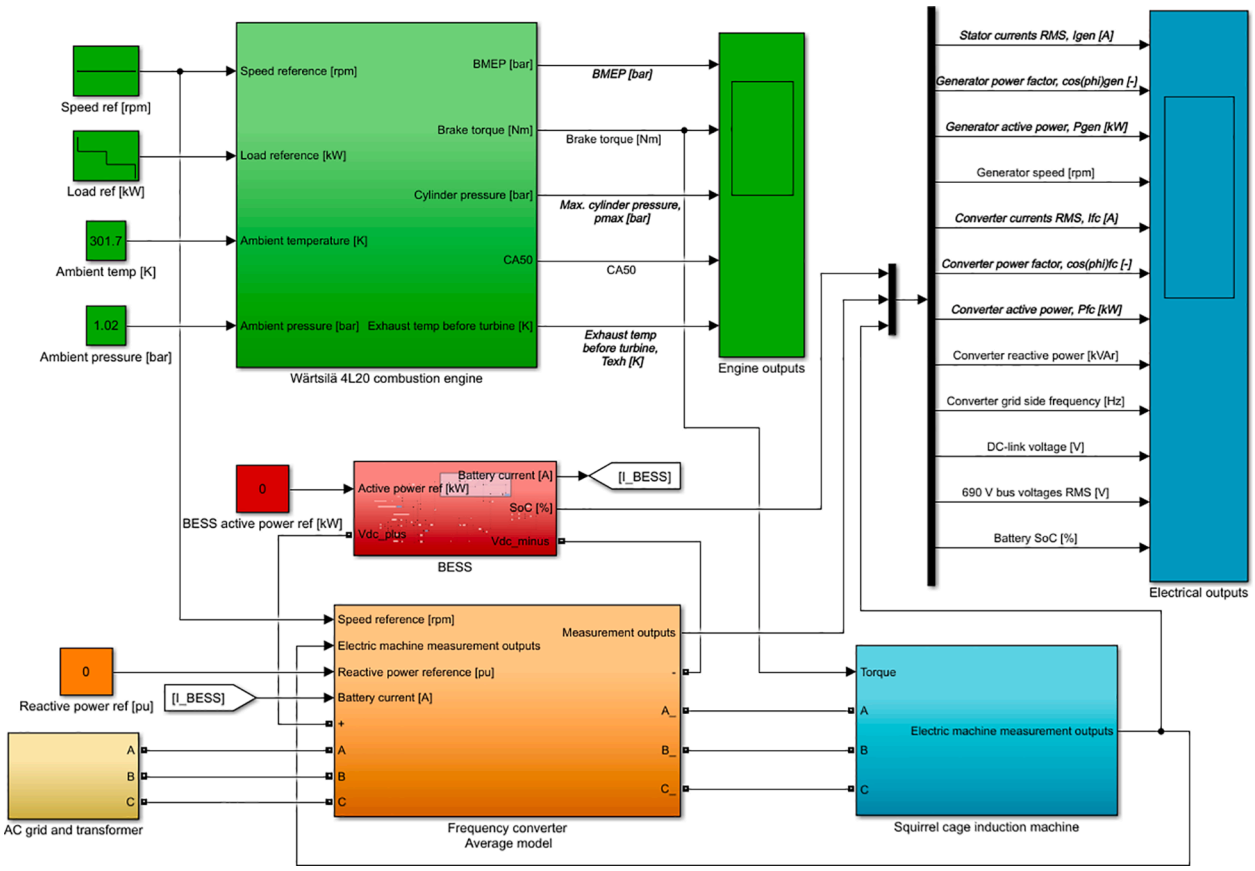

Fig. 2. General power plant model structure, including major subsystems and high-level, input–output structure. Signals later used for model validation are marked bold italic.

air path and combustion dynamics can be articulated in real-time system-level simulation, the crankshaft piston dynamics are currently not solved in favour of initiating the model with imposed speed and load references. The engine model solution provides the mechanical torque demand towards the squirrel cage induction generator (SCIG) model (blue in Fig. 2) without a feedback loop. The rotational speed setpoint is the same for both submodels.

Note, that the mechanical dynamics compared to the detailed flow, heat transfer and combustion, as targeted here, is numerically simplistic and do not pose any noticeable calculation burden. Perspective for not resolving crankshaft dynamics comes from the model calibration and validation taking the pivotal role to determine the model accuracy and calculation speed in this study. Engine tests for model validation were performed with active control of the generator's speed (+-1 rpm accuracy) to force steady-state conditions for accurate measurement of combustion indicators and thermodynamical conditions at the airpath. Hence, with the speed imposed, the engine load is determined only by the power demand (effectively fuel value injected per cycle) as input to the engine controller. This so-called "imposed speed" mode of the experimental tests is thus replicated in the model configuration. For actual control studies with the model, foreseen in the follow-up works the torque to torque coupling of engine and generator, provided by resolving the crank-shaft dynamics, will be turned on. This should be taken into account when analyzing the results of the present study.

The back-to-back FC (orange in Fig. 2) allows the engine to operate at variable speed while controlling the DC-bus voltage and reactive power introduced to the grid (yellow section in Fig. 2). To facilitate peak-shaving capability, a battery energy storage system (BESS) submodel is included (red section in Fig. 2). This system currently is not physically present in the laboratory and, as such, its model is considered generic. The BESS connects to the SCIG with positive and negative DC ports via the mentioned FC and outputs the state of charge (SoC) as a monitoring signal. The battery current is needed as an input to the FC.

In summary, the model uses speed reference, load reference, power reference and ambient conditions to calculate the condition of the grid, the battery state of charge and coupled engine torque. Note, that the scope of modelling is limited to the actual laboratory setup. As such, the auxiliary loads are not modelled explicitly, yet imposed as grid demands, as in the physical system. Fig. 4 depicts the complete input/output structure of the SCIG and FC model.

2.2.1. *The engine model*

A detailed GT-Power model was created to represent the research engine and validated in various measurement campaigns in the VEBIC laboratory. This is a one-dimensional physical model of the complete airpath, incorporating zero-dimensional combustion and map-based turbocharger submodels. The crank angle resolved combustion object imposes an experimental burn-rate shape to track the development of thermodynamical parameters in the cylinder.

The detailed model is order of seconds-fast per engine cycle, but a faster solution was required to adapt the engine model in system-level simulations in Simulink. Simultaneously, the target was to maintain the accuracy within 10% of the measured values in the most relevant performance parameters - brake power and efficiency and crank angle at 50% fuel mass fraction burned (CA50). Therefore, a fast-running engine model (FRM) was developed, using the detailed model as a baseline. The FRM implemented incremental reduction techniques to produce a lumped volume representation of the detail elements. Individual flow components were cut from 181 to 47. This, together with adjusted internal discretization lengths, reduced the total number of flow volumes to be resolved by 74%. Table 3 lists the main assumptions of the detailed 1D model and its FRM surrogate, while Fig. 3 provides the GT-Suite

Table 3
Assumptions for the detailed 1D model and its FRM surrogate.

Feature	1D-Detail	FRM
Minimum discretization length intake	50 mm	200 mm
Minimum discretization length exhaust	50 mm	300 mm
Number of flow components	181	47
Solver	explicit, forward Runge-Kutta method	explicit, forward Runge-Kutta method/explicit Euler real-time (in the RT license)
Maximum simulation time step*	0.00017 s	0.12 s
Average simulation time**	77 s per steady-state case	19 s per steady-state case (4 s with a real-time license)

*user-imposed limit.
**on single CPU (Intel i7-8750H 2.20 GHz) with 16 GB RAM.

diagram of the final FRM indicating the individual model reduction steps.

Note that in each reduction step indicated in Fig. 3, the aggregated elements were simplified in terms of accuracy, by moving from predictive, very detailed submodels of friction and heat loss to simpler approaches. This was done selectively, supported by sensitivity analysis. For example, elements of the exhaust manifold were left modelled with a predictive wall thermal solver, as it was by far the most sensitive to the accuracy of wall temperature estimation. Other elements were modelled with wall temperature imposed as an average value from detailed 1D simulations. Since the imposed combustion profile was already used in the detailed model, simplifications for combustion or cylinder elements, in general, were not required. The same holds for the turbocharger model.

Hautala et al. [26] give a detailed description of the modelling route, conversion to FRM and experimental validation. Some highlights on how subsequent model reduction steps influence model accuracy and simulation speed are provided in supplementary material D for reference.

The FRM model was finally implemented in GT-Suite-RT, an environment explicitly designed for real-time simulations such as for hardware-in-the-loop (HiL) applications. The conversion to FRM involved applying a new explicit solver which gave more direct control of integration time-step. To further shorten simulation time, the FRM's extensive input–output structure was reduced to suit the more modest needs of the system-level model discussed in section 2.2. The lumped model was converted to a Simulink S-function and incorporated into the complete power plant model (Fig. 2).

2.2.2. The SCIG model

The modelling of the SCIG and the corresponding FC (section 2.2.3) follows the approach by Domínguez-García et al. [27], with some assumptions adjusted to the particularities of the physical system described in section 2.1. This approach to modelling electrical system components is well established in other energy fields and was used, amongst others, for modelling wind power plants [28].

The main element of the SCIG model is the asynchronous machine block from the Simscape SPS library [29]. The system is described by the standard induction machine voltage equations in the arbitrary direct-quadrature (dq) reference frame. The reader is referred to the corresponding section of Simscape SPS [29] for a complete set of the governing equations.

An indirect rotor flux field-oriented control method is used, which requires the reference frame to be fixed on the rotor flux. The generator inductances and resistances are crucial parameters for an accurate SCIG representation in this case. Note that those parameters were acquired directly from the manufacturer (ABB Motors & Generators) and are

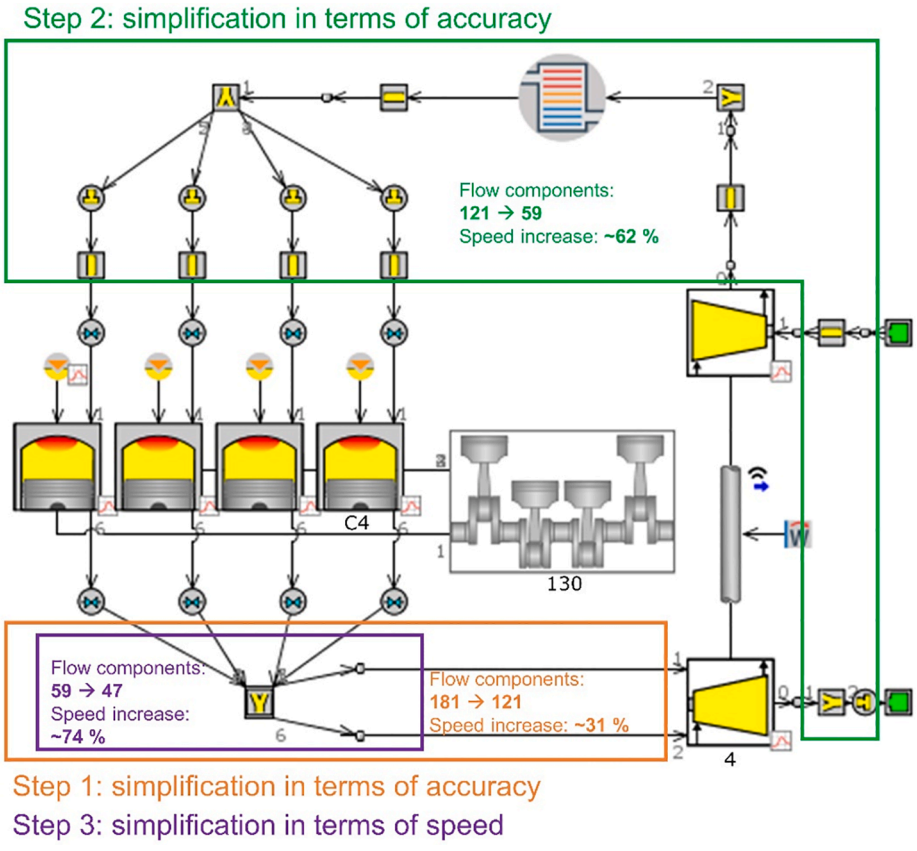

Fig. 3. GT-Suite component diagram of the one-dimensional FRM model representing the Wärtsilä 4L20 engine. The three main reduction steps are highlighted (Step 1: simplification of the exhaust manifold, Step 2: simplification of exhaust piping, intake manifold, compressor outlet pipes and intake piping, Step 3: simplification of exhaust manifold) together with the reduced amount of flow components at each step and achieved improvement in average simulation speed compared to the detailed model.

considered accurate. Other parameters relevant to model identification are in the supplementary material C and in the corresponding discussion in section 2.1.2. Fig. 4 illustrates the input and output structure of the SCIG and its relation with other elements of the electrical system, described in the following subsections.

2.2.3. The FC control

The IGBT bridge available in the Simscape library does not meet this studýs real-time requirements, so it is replaced with an average converter model (Figs. 4 and 4a). This is represented by equivalent voltage sources generating the AC voltage, averaged over one cycle of the switching frequency. Note that a trade-off of using the average model instead of the detailed, switching-frequency approach, is that harmonics are not represented [30].

Following Domínguez-García et al., [27] the DC-link voltage is determined as the time-awarding integral of the respective grid ($I_{DC,grid}$) and stator currents ($I_{DC,stator}$). When the BESS is included in the model, the DC-link equation needs to take into account the current going to (or from) the battery (I_{BESS}), resulting in Eq. (1)

$$V_{DC} = V_0 + \frac{1}{C_{DC-link}} \int_0^t (I_{DC,grid} - I_{DC,stator} + I_{BESS}) dt. \quad (1)$$

where V_0 is nominal voltage in the DC-link and $C_{DC\text{-}link}$ denotes the corresponding capacitance (supplementary material C).

The converter model further consists of submodels for the generator-side converter control (Fig. 4c) and grid-side converter control (Fig. 4b). The principles of these control models are summarised below and Fig. 4 shows their corresponding inputs and outputs.

Generator-side control is by independent control of flux and torque through the control of independent stator current d-q components. The rotor flux is estimated and calculated from the machine equations, enabling sensitivity to the motor parameters [27]. This control strategy is implemented using the Simscape SPS Electric Drives library blocks, including the: (i) Speed Controller (AC); (ii) Field-Oriented Controller (FOC), and (iii) Inverter (Three-Phase). The speed controller block needs a speed reference signal (rpm) and the actual rotor speed (wr_SI). These inputs are depicted in Fig. 4c: inside the same figure are the outputs of torque reference and flux reference signals to the FOC. In addition to the torque and flux references, the FOC also needs the stator currents (Iabc_stator) and the rotor speed (wr_SI). The FOC will then provide control signals to the average three-phase, built-in inverter. For this specific control system, it is important to choose the rotor flux rotating reference frame for the asynchronous machine block. The rotor flux position and magnitude are needed for indirect rotor flux control. They need to be estimated by means of the machine parameters and measured stator current. The supplementary material C lists the values assumed in this research.

Grid-side control is by active and reactive power control of independent grid current d-q components. Hence, its function is to keep a constant DC-link voltage while controlling the active and reactive power injected into the grid. [28]. The grid-side control system is based on the corresponding system from MathWorks example model [30]. Control systems utilising sinusoidal voltages and currents usually are not preferred in system-level simulations. Instead, the use of steady values simplifies the control design and related mathematics. Accordingly, the time-dependent voltages and currents can be transformed to a reference frame rotating with the grid frequency, in which they appear as constants, with the condition that their frequency is equal to the frequency of the reference frame. In the stationary reference frame, they appear as sinusoidal parameters that vary with the grid frequency. [31]. A phase-locked loop (PLL), inside Fig. 4b, is used to synchronise the grid-side converter voltage output with the grid. For the PLL, the grid voltage frequency and angle need to be detected from the input signal Vabc_grid [32]. The DC-link voltage reference and reactive power reference values are needed for determining the current references, which in turn determine the voltages to be applied in the grid side.

2.2.4. The BESS model

Fig. 5 depicts the complete BESS model. Its core is the Li-ion battery model from the Simscape SPS toolbox [33]. This is an equivalent circuit battery representation which resolves battery current, voltage and SoC. The SoC is given as a relative value (0–100%) and here is calculated by current integration according to Eq. (2) [33]:

$$SoC = 100\left(1 - \frac{1}{Q}\int_0^t I_{BESS} dt\right). \quad (2)$$

Here Q is the maximum battery capacity in Ah and I_{BESS} is the battery current already identified in Eq. (1). The battery model is parameterised with nominal voltage and rated capacity (supplementary material C) and scaled to the energy capacity of 300 kWh for this particular case study.

The BESS accommodates the battery management system (BMS), which protects against overcharge and deep discharge. Rapid peaks in current are likely to damage the battery and so the model uses a ramp rate limiter [34]. Furthermore, the BMS model follows the active power reference as long as the SoC is within the given limits. Consequently, if

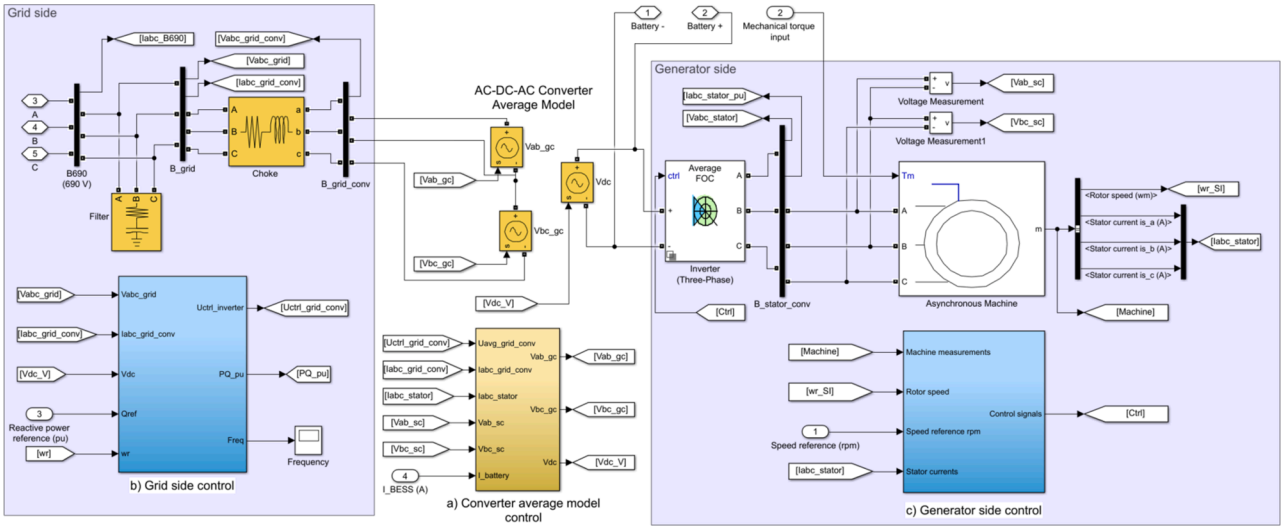

Fig. 4. The SCIG model, together with the FC and its control on generator side and grid side.

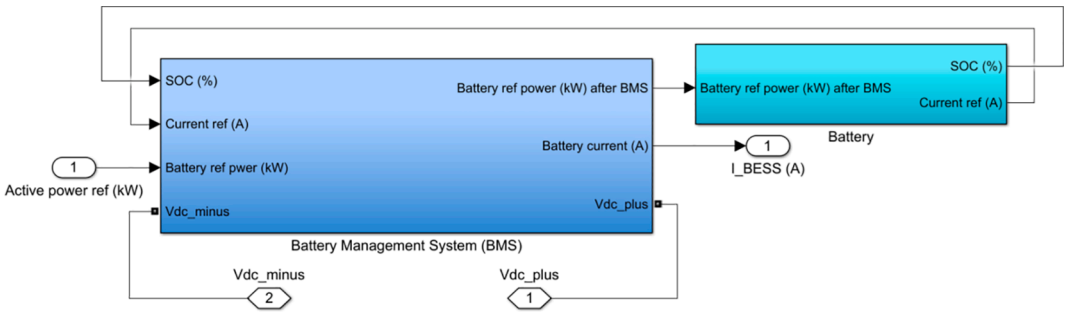

Fig. 5. The BESS, divided into the battery model and BMS model.

SoC is below 20%, the battery is only allowed to charge and a power setpoint that requires discharging will be ignored. Similarly, if SoC is above 90%, the battery is only allowed to discharge. The maximum power exchange is arbitrarily limited to 1000 kW to ensure that the FC capacity is not exceeded.

The BESS is connected to the FC DC-link through a bidirectional DC-DC converter. Here, the DC-DC converter is represented in a simpler way, avoiding switching phenomena. A power reference is fed to the BESS and then divided by the battery measured voltage, resulting in a reference current. The battery output power is similarly divided by the DC-link voltage. This results in the current I_{BESS} which is injected into the DC-link using a controllable current source.

2.2.5. *The Simulink and GT-Suite interface*

In the final step for implementing the system-level power plant model, the GT-Suite engine model was imported to Simulink. GT-Suite provided instructions for establishing the connections between the two software and they also provided all the necessary files for the code generation of the engine model. Thus, GT-Suite provided a Simulink real-time block library explicitly designed for performing Simulink Real-Time simulations including GT-Suite models.

The first step was to create a data file of the engine model in GT-Suite, this data file was used as an input parameter to the Simulink block "GT-SUITEv2020.0RT with In-Cylinder Pressure" which is an S-function. This block was provided by GT-Suite and is used for creating the link between the software. Other parameters that the block needs are sample time, number of inputs and number of outputs. These are the number of inputs and outputs that are exchanged between the GT-Suite engine model and Simulink. Other files provided by GT-Suite included C source code, header files and object file library files that are all needed in the code generation of the engine model, for creating the real-time application that is capable of running on a target machine.

2.3. *Model calibration/validation methodology*

Since the models developed here are physics-based, they do not require broad training data. This ultimately forms one of the advantages of such approaches over the black-box/data driven models. The predictive nature of the model should handle the performance outside the calibration matrix. The following validation (on the full operating envelope) is also a final test of this predictivity (performance outside of the calibration area), hence the validation of the whole thesis regarding the physics-based nature of the model.

The calibration procedure generally follows the "from detail to general" principle. First, governing components (submodels) of the combustion system (cylinder, charge air-cooler, turbine, compressor, etc.) and the electrical system (generator, frequency converter, etc.) were calibrated separately with imposed measured inputs. Then, the combustion engine model and the electrical equipment model were calibrated and validated separately, decoupling the variables and avoiding error transfer from one to the other. The real-time engine model validated in GT-Suite was further imported to Simulink and in that way, the combined model could be simulated and validated.

Exhaustive discussion of a complex procedure of calibrating physics-based engine models against experimental results, one can find in an excellent work by Rolf Isermann [35] or in the GT-Power application manual [36]. The calibration process for the engine model explored here, has been thoroughly documented in the earlier work by Hautala et al. [26]. The present work builds on this and focuses on validating the real-time FRM versus its full-fidelity counterpart. This was done for four representative load points corresponding to the validation space of the electrical model discussed below and includes only the selected variables relevant for system-level simulation. Table 4 lists the key parameters included in the engine modeĺs final validity check, together with their tolerance levels.

The electrical model was calibrated at nominal operating conditions for the generator (Table 2). Overall controller parameters were tuned to fit the model to the experimental data. This included speed controller PI parameters, flux controller PI parameters and the DC-link capacitor value (which could not be identified from the technical sheets). The supplementary material C lists all the calibrated parameters. The tuned model was finally validated over four representative operating points related to the active power setpoints (200 kW, 370 kW, 600 kW and 750 kW). The active power setpoint or load reference value is the active power output that is expected from the generator. Note that although the FC enables variable speed operation, the experimental data gathered from the existing laboratory infrastructure were obtained only for the combustion engine running at a constant speed of 1000 rpm.

Six experimentally measured parameters were selected to validate the electrical model output. These are direct outputs deriving from the generator and FC, as shown in Table 4. For the quantities measured directly, respective device accuracies were used as restrictive tolerance indicators [37,38]. The tolerance level for the engine quantities, which were measured indirectly, was calculated based on measurement accuracies of the inputs, using the partial divertive method. Refer to the original work by Kline and McClintock [39] for details of experimental data uncertainty estimation.

The same parameters are in principle used to validate the combined electric-combustion power plant model. Assuming that the engine model already has been validated separately, this is sufficient to conclude the discussion of the system-level model validation. Note that the BESS model is not part of the validation methodology described above: the battery module was not operational at the laboratory when the validation tests were performed. The BESS model is considered generic and due to its mathematically simple structure does not require any calibration. Nevertheless, dedicated simulations have been performed in order to establish that the BESS control worked as expected. Battery reference power was varied to replicate typical charge–discharge characteristics, over the overall simulation time of 1500 s. Battery SoC and system output power were then analysed to determine model feasibility.

Table 4
Parameters measured for model validation, along with their respective tolerance levels.

Level	Name	Symbol	Unit	Reference data	Tolerance	Corresponding model location
Engine	Break mean effective pressure	*BMEP*	bar	detail 1-D engine model; accuracy within cylinder-to-cylinder variations	0.5 bar	CrankTrain 130 (Fig. 3)
	Max. cylinder pressure	p_{max}	bar		5%	Cylinder C4 (Fig. 3)
	Exh. Temp. turbine inlet	T_{exh}	K		5%	Turbine 4 (Fig. 3)
Generator	Output power	P_{gen}	kW	direct measurement: generator protection relay REG615	1.5%	Calculated from I_{abc_stator} and V_{abc_stator} in Fig. 4
	RMS current	I_{gen}	A		0.5%	Calculated from I_{abc_stator} in Fig. 4
	Power factor	$\cos(\phi)_{gen}$	–		1.5%	Calculated from generator active and reactive power which are calculated from I_{abc_stator} and V_{abc_stator} in Fig. 4
FC	Output power	P_{fc}	kW	direct measurement: power monitoring unit Vamp 260	1%	Calculated from active-reactive power per unit vector PQ_pu in Fig. 4
	RMS current	I_{fc}	A		3%	Calculated from I_{abc_B690} in Fig. 4
	Power factor	$\cos(\phi)_{fc}$	–		2%	Calculated from active reactive power per unit vector PQ_pu in Fig. 4

2.4. Remarks on real-time methods

A digital twin in this paper refers to a real-time simulation capable model of the power plant in VEBIC that through the Speedgoat I/O module can communicate with its real-world power plant counterpart in real-time. The main challenge in this implementation is the trade-off between simulation speed and accuracy outside of the nominal operating range (predictivity) which we aim to secure with a physics-based engine model.

Towards this goal, after the combustion engine and electrical elements of the model were successfully individually validated in terms of target accuracy and real-time simulation capability on a desktop computer, the next step is the final validation of the combined models on a real-time target machine. In this case, the target computer (Fig. 1-j) was a Dell OptiPlex 760 from 2008, with a four-core CPU and 8 GB RAM, running a Simulink Real-Time 2017a kernel. In principle, the digital twin needs a real-time feed of measured data from its physical counterpart. To enable this, the target computer communicates with the Speedgoat machine (Fig. 1-g) which controls the real engine, through the Modbus protocol and the Speedgoat Simulink driver blocks [40]. Note that this parallelisation assures that the digital twin can function redundantly without the risk of overloading the essential control function of the Speedgoat.

Aside from the above hardware constraints, the target machine implementation imposed relevant changes to the solver. The target simulation in Simulink Real-Time employs a discrete solver, giving direct control over model execution by imposing a fixed time-step. The user can therefore adjust the simulation time-step to match the application demands and available computational power, while avoiding stability issues imposed by the Courant condition [41]. Solver choice was therefore the most fundamental change compared to offline desktop implementation.

3. Results and discussion

These are the validation results of the calibrated models that comprise the complete power plant model. The sequence of validation started with the decoupled engine and electrical component models, and concluded with their co-simulation in a desktop environment. Presenting the results in the same order aids comprehension of the error transfer issues relating to the complete power plant model. Following successful desktop validation (subsection 3.1) the proof of concept of the digital twin has been tested on the real-time target computer and those results are discussed in subsection 3.2.

3.1. . Desktop validation

3.1.1. Validation of the engine model

Engine performance parameters considered during validation were BMEP, averaged maximum cylinder pressure and exhaust temperature before the turbine. Additionally, the real-time factor was used as a simulation speed indicator. To this end, Fig. 6 shows the steady-state simulations performed with three versions of the model: the detailed model that serves as a reference, its FRM surrogate and the final real-time FRM that was later coupled to the full power plant model. Extended insight on model validity in subsequent reduction steps can be found in supplementary material D.

Analysis of Fig. 6 shows that the FRM cuts simulation time by an order of magnitude when compared to the detailed engine model. Importantly, its predictive capability in terms of relevant performance parameters remains virtually unchanged. The accuracy loss in this step is minor, mostly within the 5% tolerance levels set for the governing outputs. The largest deviations appear at low-load conditions, where air-path pulsations seem to play the largest role. However, the effect is only significant for exhaust temperature, which does not exhibit stiff coupling with the electric model. To this end, the primary input–output relation between the combustion engine and the whole power plant is through BMEP, as evident from Fig. 2. Brake torque is derived from BMEP by scaling with cylinder dimensions and engine speed. This quantity is conserved with superior accuracy with respect to both the detailed model (Fig. 6) and the actual physical engine outputs [26]. Fig. 6 shows that the reduced-order FRM, without a tailored solver, remains on the borderline of real-time capability, with real-time factors varying on a case-dependent basis from 0.9 to 1.9. Further applying a new explicit solver optimised for speed (GT-Suite-RT licence) reduces the FRM's real-time factor to 0.35 on the desktop PC, proving its suitability for digital-twin implementation. Explicitly, the solver cuts down the simulation time to below 4 s for the 50 engine cycles required to attain steady-state conditions in this trial run. This is over 70% faster than the baseline FRM and the simulation time is almost 90% shorter than the detailed engine model. Naturally, such simulation times are below typical engine air-path response times considered in this research.

Interestingly, compiling the FRM using the real-time version of GT-Suite has almost no impact on model accuracy. This is evident from Fig. 6 and so does not require further comments. It is suffice to say that both the stand-alone desktop FRM and its real-time-executable compilation are well within the targeted accuracy limits.

3.1.2. The power plant model without BESS

Fig. 7 presents the relevant electrical outputs of the power plant model at the same four operating load points used for the engine model (Fig. 6), and sets them against the corresponding laboratory measurement results. The simulated results are presented for the decoupled

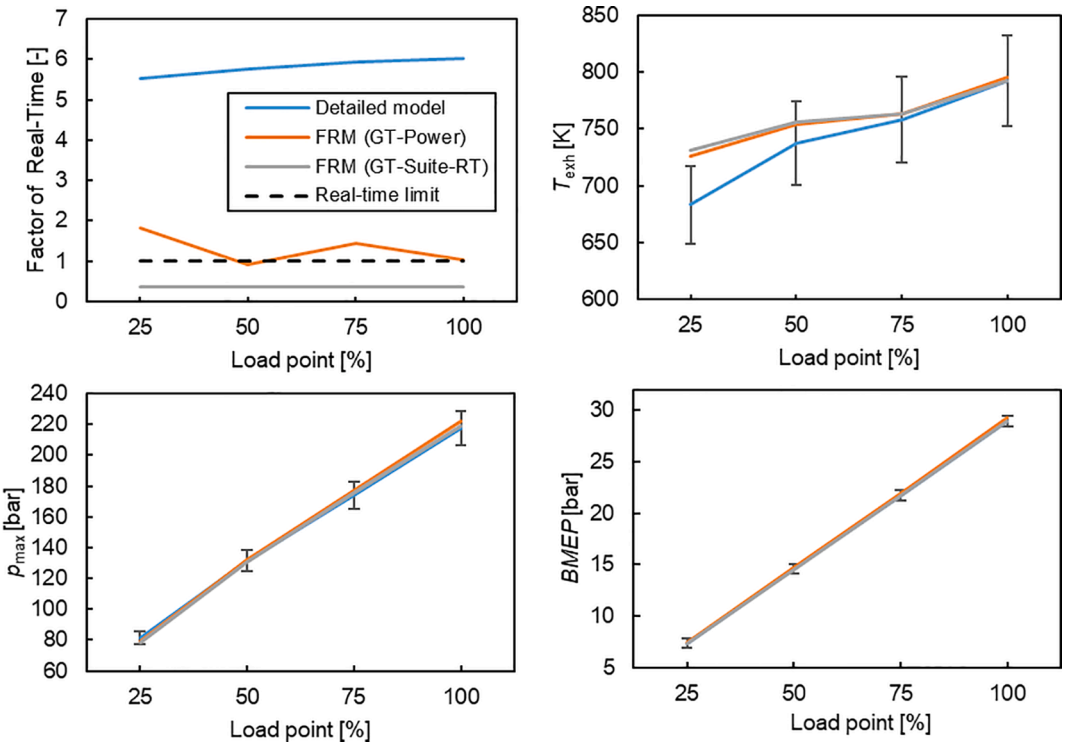

Fig. 6. Validation plots of the FRM and its real-time version against the simulation results of the detailed engine model. The error bars are the imposed tolerance levels in Table 4.

electrical system (calibration model) and the electrical system coupled with the calibrated engine model. In the first case, the power plant model was fed with imposed exact engine load reference values to decouple the engine model-related errors.

When considering the generator element of the decoupled electrical model, the simulation results in Fig. 7 (blue bars), are close to the corresponding measurement results. The active power is within the measurement accuracy for all cases except the 200 kW point. The simulated RMS current is slightly beyond this restrictive threshold. Note, however, that here the simulation value is within the standard deviation of the measured RMS current. Given the steady-state nature of this validation endeavour, the generator model gives an accurate representation of the actual SCIG in the vast majority of the operating envelope. The exception is the low-load point (200 kW), where the simulated generator power factor ($\cos(\varphi)_{gen}$) is overestimated. The used machine resistances are for specific stator and rotor temperatures and the lowest load point may be insufficient to reach those running temperatures, manifesting in greater inaccuracies in the simulation values.

Note, that the power factor of the FC is held sharp at a value of 1, regardless of the operating point. This is equally true for both the measured and simulated values and can be attributed to an effective grid-side control system. The system delivers unity power factor to the grid, both in the model and in the laboratory setup. As the results are trivial they are not shown explicitly in Fig. 7.

Further discussing the standalone electrical model, the simulated converter-side currents and powers differ more significantly from their measured references. This can be partly explained by the fact that the requirement for real-time simulation means the FC is represented as a simplified average model. As for the generator, the low-load point shows the biggest deviations. The simulated power is around 17% higher than the corresponding converter output. Note that in reality, the FC with nominal power of 2000 kW has an efficiency of around 97% at its nominal point, but efficiency is lower for the load range presented here. The average model used here does not properly consider these effects, hence the resulting overestimation. The efficiency losses become a smaller proportion of the power produced at high loads, so the relative differences between simulated and measured results diminish to 6.5%, 3.9% and 3.0% respectively for 370 kW, 600 kW and 750 kW loads. The absolute delta between the simulated and measured results is almost constant across the load sweep for both the converter power and its RMS current. This means that the trends are predicted correctly, and the model is suitable for control purposes. Furthermore, the constant deviation can be eliminated easily if an additional tuning parameter is introduced to the average converter model.

Co-simulating the electrical and combustion engine models causes overestimation of all the parameters on the electrical side (Fig. 7 grey bars) at partial loads. The deviation statistically increases towards the highest loads, reaching 3% for both generator and FC power outputs. Similarly, at the lowest load point the combined power plant model deviation rates are slightly lower than the decoupled electrical model, although the differences between the two are barely noticeable at this point. The above are straightforward effects of the engine torque error transfer from the combustion model. Note, that BMEP (as torque derivative) is overestimated at higher loads for the reduced-order engine model. As this might seem marginal for the detail model vs. FRM comparison in Fig. 6, the detailed model itself carries a maximum 2% inaccuracy versus the measurement results. Again, the reader is referred to the work by Hautala et. al [26] for detailed elaboration of engine model errors.

Note that later when actual control studies are targeted with this power plant model, the engine model should include the torque feedback from the generator as an input in order to enable the so-called load mode engine control. This load feedback input is provided by resolving the crank-shaft dynamics. In this system simulation setup, the engine is in the so-called speed mode to replicate the experimental conditions of steady-state performance tests. This method typically provides steady-state results very quickly because the speed of the engine is imposed for the duration of the simulation, thus eliminating the relatively long time that is required for the crankshaft speed to reach steady-state in a loaded engine (usually around 500 cycles).

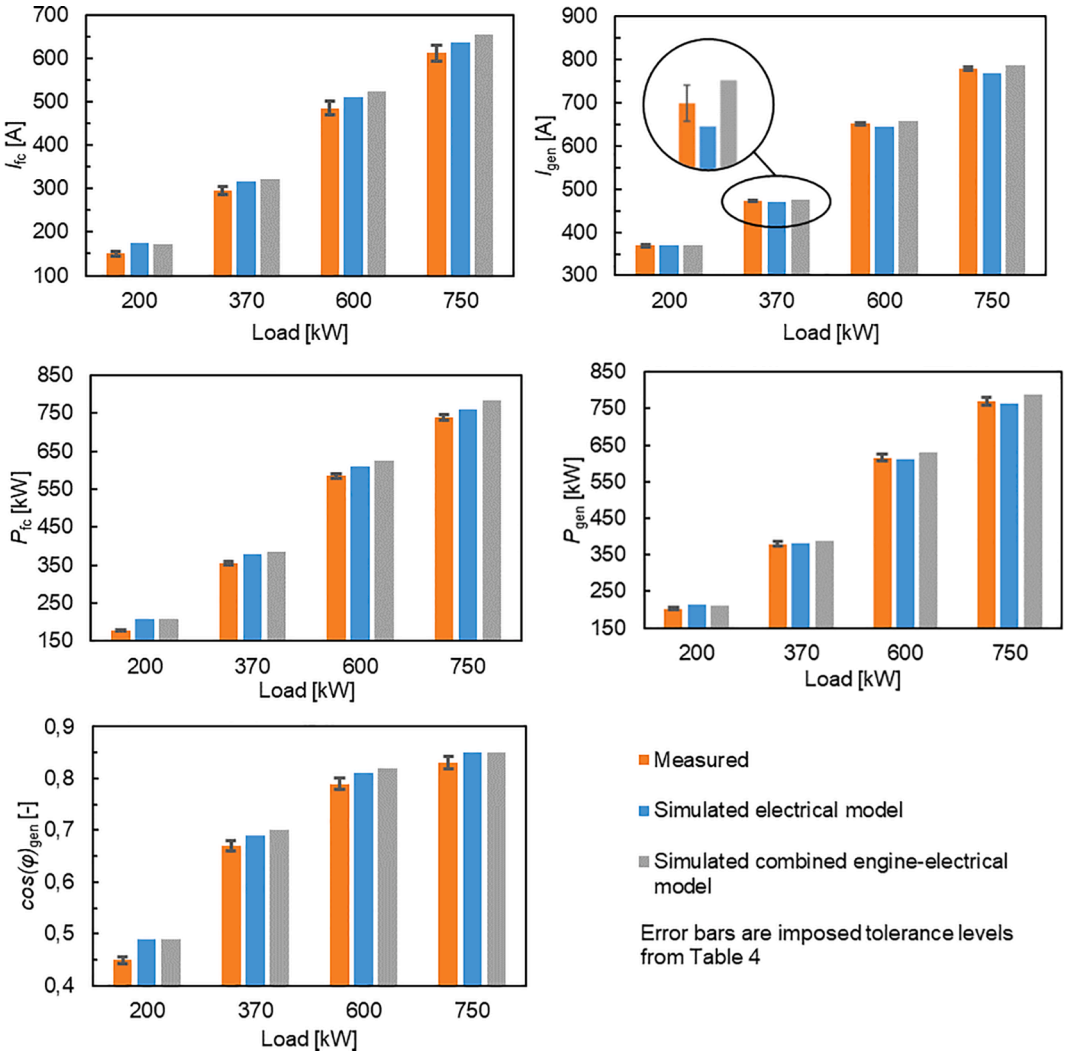

Fig. 7. Results of validation of the electrical system (excluding BESS) for the four load points: 200 kW, 370 kW, 600 kW and 750 kW.

3.1.3. Functionality check of the BESS model

The battery energy storage system was not installed in VEBIC when this research was performed and therefore its model could not be validated using direct experimental results. Fig. 8 presents the results of a functionality check of the BESS model coupled to the plant model. This check sought the correct response for the active power reference signal (input value no.1 in Fig. 5). As shown in Fig. 8, the reference signal was a step excitation changing from 0 to 1000 kW at 100 s of the simulation, dropping to −1000 kW after 500 s. Other set-points for engine speed and engine load reference were kept constant, at 1000 rpm and 800 kW respectively, across the whole 1500 s of simulation.

Fig. 8 shows that the BESS model is working correctly. The battery stops charging when the SoC reaches 90% and stops discharging when SoC drops to 20%, as programmed in the battery management system. Between the SoC limits, the battery immediately responds to changes in the active power reference. The total output power at the point between the FC and the transformer equals the sum of the generator output and the battery energy storage output. It can be seen that when the BESS is

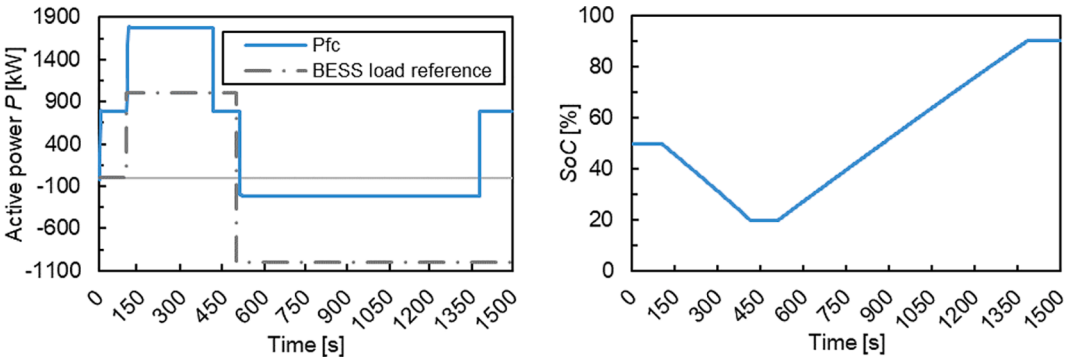

Fig. 8. The active power output at the point between the FC and the transformer, P_{fc}, the BESS load reference and the battery *SoC*.

discharging with 1000 kW active power (reference), the systems total output power at the point after the FC is 1780 kW. Note that the positive value of output power means that the energy flows into the main AC grid. When the battery is discharged below 20% SoC at approximately 400 s, it rejects the power setpoint and the total active power output of 780 kW comes solely from the generator. At 500 s the BESS reaches a new setpoint at −1000 kW, resulting in a total active power output of −220 kW. This means the battery is charging using approximately 780 kW from the generator and 220 kW from the grid. Finally, when the battery is fully charged, the total active power output will be 780 kW once again.

3.1.4. Intermittency balancing with the combined engine-generator-BESS power plant model

A combined combustion engine and battery storage power plant can be used for several applications in the stationary power sector. Such applications include among others peak shaving, ramp support, voltage support and frequency regulation. In this section, intermittency balancing is showcased, demonstrating the functionality of the model for handling power fluctuations in the grid. Such fluctuations are commonly associated with large scale integration of renewable energy sources rendering fast-response power plants necessary.

In this showcase, the engine operates at its nominal power, translating to 788 kW as the generator output. The fast-acting BESS handles the rapid intermittency balancing by charging and discharging accordingly. Fig. 9 shows the input active power reference, which is the power requested by the grid and the outputs active power P_{fc}, P_{gen} and battery *SoC*.

From Fig. 9 it is seen that the battery is charging when the grid power demand is below 788 kW on the generator shaft and discharging when the grid power demand is above 788 kW. The results prove that the BESS can tackle the intermittency balancing. Note, that the engine output and hence generator active power output P_{gen} is kept constant as an illustrative limit. When the grid power demand is more than P_{gen}, the battery needs to provide for the additional grid demand which manifests in decreasing battery *SoC*. Similarly, when the grid demand is less than the P_{gen} value the battery will store the extra power and it charges, increasing the *SoC*.

It can be further observed from Fig. 9, that the active power output from the frequency converter (P_{fc}), is following the grid requested active power reference as intended. The battery reacts to power reference changes immediately when its SoC is between upper and lower limits, 20% and 90%. Note that the positive value of output power, P_{fc}, means that the energy flows into the main AC grid. Note, that in this case study, only 500 s was simulated and fairly fast changes were imposed for the grid requested power reference. In actual inclemency balancing application additional control features need to be considered to handle the system behaviour at boundary conditions (for instance SoC approaching maximum or minimum values). However, this first demonstration was mainly intended as a use case example, and the energy management system optimization is an object of further research.

3.2. Simulations on the target computer

In the real-time simulation, the model parameters are updated synchronously with the real-world input. Hence, digital twins must use a fixed-step discrete (without continuous states) solver. The minimum step size depends on the computational capacity of the target machine. A time-step that is too small will cause an overrun because the target CPU will not be able to process the model in the time available. On the other hand, increasing the step size detracts from accuracy and leads to potential aliasing effects. Hence, the challenge is to find a suitable compromise between accuracy and speed [42]. This has been investigated for both the engine model and the electrical system model separately.

3.2.1. The engine model

The average task execution time (TET) for the engine model on the used target computer was 0.807 s. This was an order of magnitude slower than for the desktop simulations. It should be noted that the target computer had considerably lower computational power than the desktop PC (Intel Core Q9400@2.66 GHz CPU/8 GB RAM vs Intel Core i7-8750H@2.2 GHz CPU/16 GB RAM respectively). Bearing in mind this limited computational performance, the real-time simulation of the engine model was performed with an imposed sample time-step of 1 s. This step is too long to capture the detailed dynamics of the in-cylinder processes, yet still in range of typical airpath response times. This is confirmed in Fig. 10, which shows the sample load transient throughout 200 s. The results here were post-processed in Excel for better quality: the actual Simulink Real-Time output is provided for reference in the supplementary material E. The load and start of injection (SOI) in Fig. 10 are inputs to the model. The SOI angles are part of the engine control map and are adjusted by the injection controller for best performance at different engine load conditions. Consequently, the resulting crank angle of 50% fuel mass fraction burned (CA50) that influences overall engine efficiency, and exhaust temperature before turbine, were considered as model outputs (responses) in this test case. The output BMEP is calculated by the model directly from the in-cylinder pressure. Additionally, BMEP recalculated from model inputs is shown as a reference.

The model failed to reproduce the in-cylinder pressure because the sample time was too large to catch the rapid combustion timescale, resulting in aliasing effects. Cylinder pressure is not shown explicitly in Fig. 10, but one effect of the models shortcoming in this regard is unrealistic (oscillating) behaviour in exhaust temperature. It should be noted, however, that the mean values of BMEP and CA50 derived from in-cylinder pressure are conserved. Results of their real-time calculations match the desktop simulations 1:1, except at the load transition points, where the deviation in CA50 did not exceed 2%. The same holds for the exhaust temperature. The time-averaged exhaust temperatures

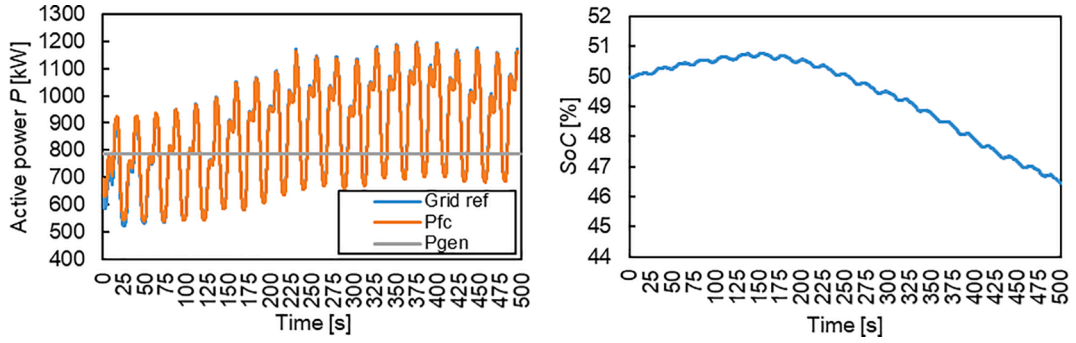

Fig. 9. Grid intermittency balancing handled by a combined engine-BESS power plant is demonstrated by showing the grid requested active power reference, the active power output at the point between the FC and the transformer, P_{fc}, the generator active power output P_{gen} and the battery *SoC*.

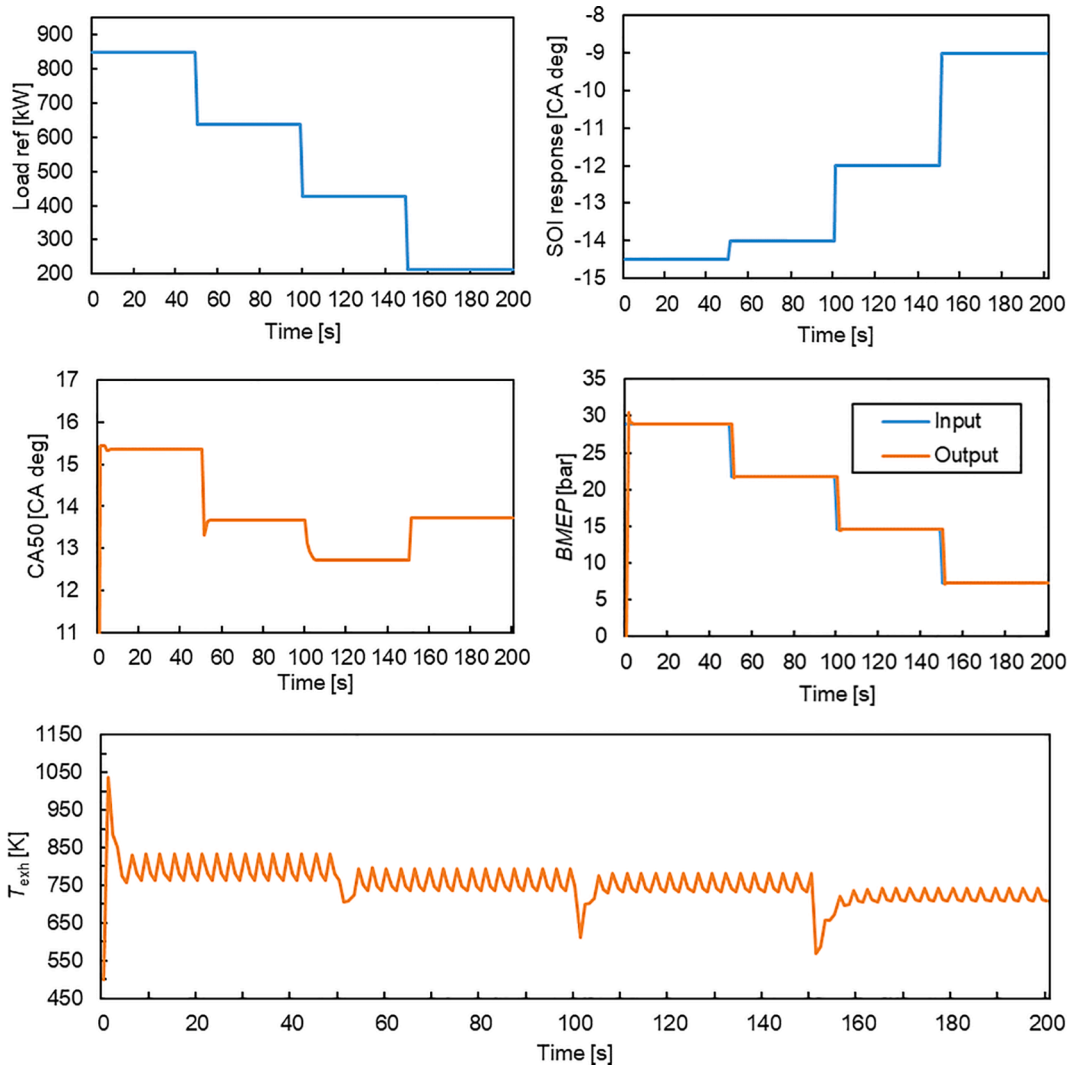

Fig. 10. Simulated engine model inputs and outputs during 200 s of real-time simulation. The sample time was 1 s.

over subsequent load points are within 5% of the desktop model predictions.

3.2.2. *The electrical model*

To verify the real-time performance of the electrical equipment model, it was run on the target computer using Simulink Real-Time. The maximum and minimum TETs were 30 μs and 3 μs respectively. The electrical model is capable of real-time simulation, with a sample time as small as 50 μs.

Fig. 11 shows the system's real-time reaction on mechanical torque input coming from the engine (imposed in this exercise). The system reaction is correct and the relevant power and current indicators converge to the same steady-state values (within the adopted tolerance levels) as for the desktop simulation. Refer to Fig. 7 for comparison. Note that the simulation results were post-processed in Excel and here the simulation was started from steady-state. Otherwise, due to the starting of the SCIG, time constants and relatively slow regulators, it would take tens of seconds to reach steady-state.

Fig. 11 shows that the model outputs P_{fc}, I_{fc} and $\cos(\varphi)_{fc}$ in the real-time simulation were converging to the same values as in the corresponding desktop simulation shown in Fig. 7. For instance, the active power output from the FC (P_{fc}) in Fig. 11, converged to 760 kW, 609 kW, 378 kW and 209 kW at corresponding steps of the torque input. Similarly, the error in I_{fc} values, converging to 636 A, 510 A, 316 A and 175A respectively in real-time simulation. The desktop simulation gave exactly the same values as the real-time simulation on the target PC, because the same sample time 50 μs could be used also for real-time simulation without experiencing CPU overload. Finally note that, according to Fig. 11, the power factor delivered to the main grid ($\cos(\varphi)_{fc}$) was held at 1 regardless of the operating point, indicating the well working grid-side control. This, along with other results discussed here, proves that the electrical system model meets the requirements of digital twin implementation without restrictions.

4. Discussion - towards the full physics-based power plant digital twin

Fig. 12 illustrates the main steps taken towards creating a complete physics-based power plant digital twin. The code generation and downloading to target machine have been successfully implemented for both governing system models (combustion engine and electrical system) as well as for the combined power plant model. Considering the engine modeĺs shortcomings discussed in section 3.2.1, the combined engine–electrical equipment model was not real-time capable. The large computational demand of the physics-based engine model meant that the coupling resulted in a model that was too heavy for real-time simulations on the target computer and consequently no communication could be established with the physical counterpart in VEBIC (Fig. 12).

Note that to reduce the computational burden, we had utilized different dynamics in the engine model and the electrical part model,

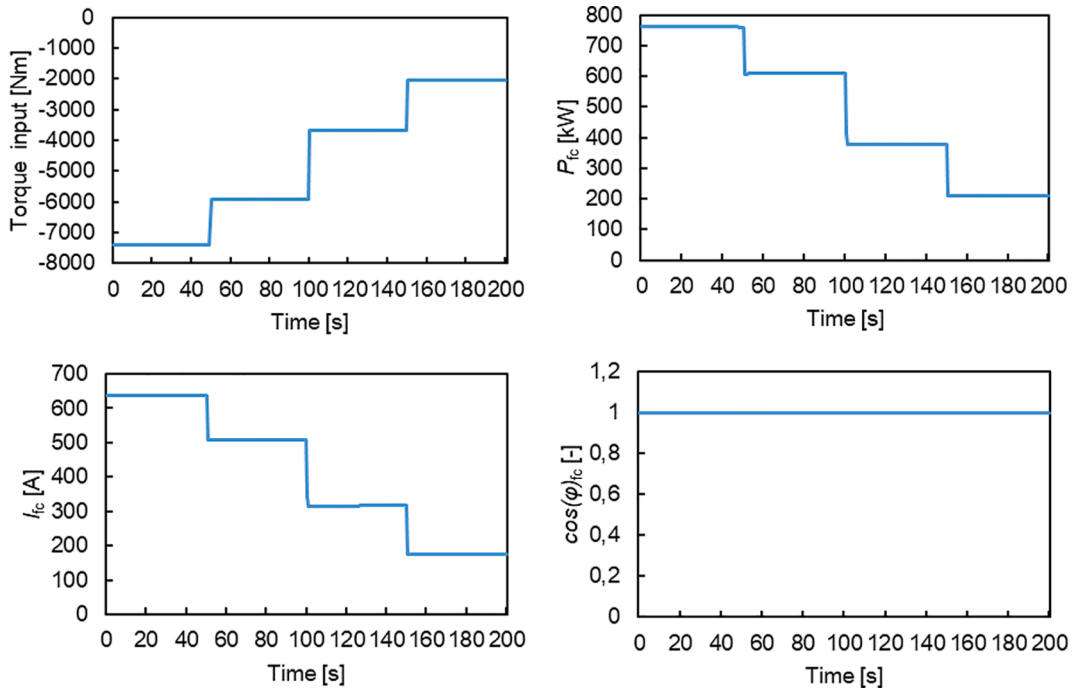

Fig. 11. Electrical model inputs and outputs during 200 s of real-time simulation; sample time was 50 μs. After over 30 h of continuous real-time operation, the model did not cause any CPU overruns.

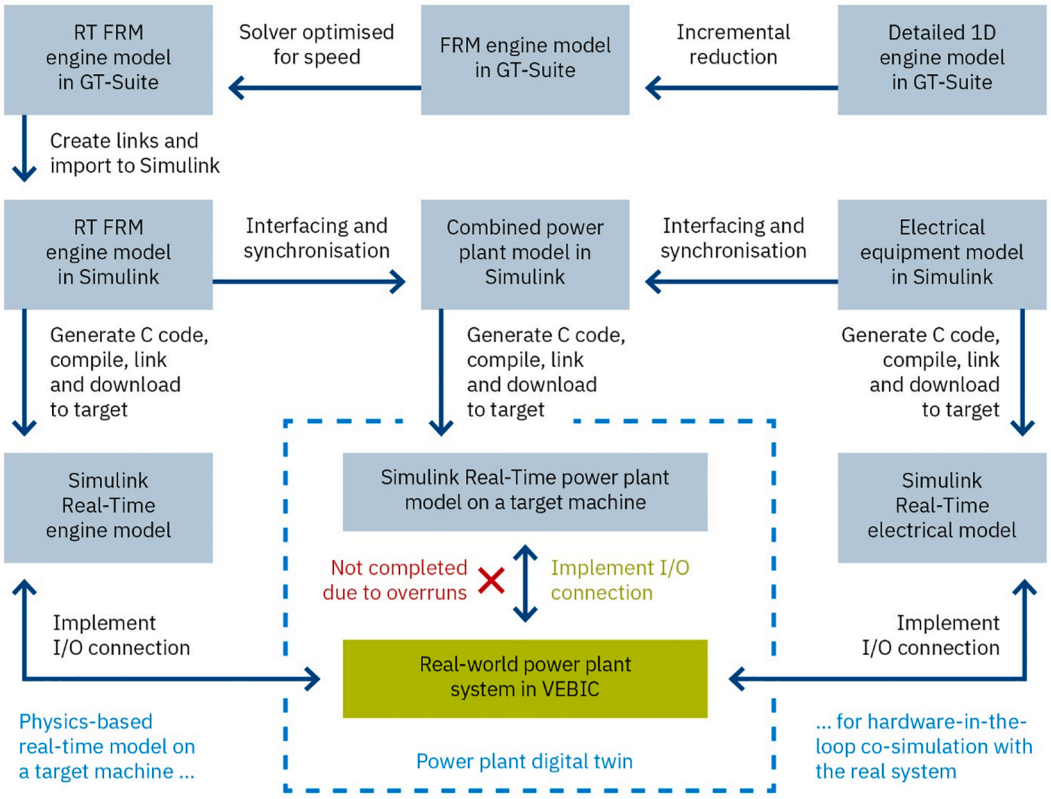

Fig. 12. The process of creating a physics-based power plant digital twin followed in this work. The X marks the point where the overruns occurred and hence the obstacle to be able to implement the real-time communication and perform hardware-in-the-loop co-simulation with the real-world power plant in VEBIC.

allowing the submodels to run with different sample times in co-simulation. The engine model had a sample time of 1 s, while the electrical system model used a significantly smaller sample time of 50 μs. For ensuring correct data transfer between subsystems with different sample times, rate transition blocks were used. In addition, the tasks were allowed to execute concurrently on the target. To this end, distributed computing was utilised and tasks with different sample times were run on different cores in the target PC. Still, with the legacy hardware

available in this project the solution was not enough, due to the low number of cores available on the target machine and the overhead for inter-core communication.

Consequently, further incremental reduction of the engine FRM is considered necessary for progress towards a whole system-level digital twin. Resolving the instantaneous in-cylinder pressure trace is the most computationally demanding part of the FRM, but this function can be substituted with a mean-value combustion model, where relevant performance factors are correlated over the engine cycle to relevant sub-inputs. The model is thus still fully predictive in terms of airpath (except second-order pulsations) and semi-predictive in terms of combustion. Depending on the quality of calibration, this simplification does not necessarily bring further inaccuracy, but compromises validity range (model cannot extrapolate) and level of insight (no in-cycle control, just cycle-to-cycle basis). However, the approach excels in simulation time, and is likely to be as fast as the current electrical model. Thus, the following steps are necessary in moving towards a full physics-based power plant digital twin: (i) calibrate the mean-value combustion model, basing on the current FRM implementation, and validate it for accuracy and validation range; (ii) implement co-simulation with the electrical part, including out-of-range safeguards for the mapped combustion; (iii) validate the whole model for real-time capability and accuracy against the targets imposed by actual use cases of the power plant digital twin. If these three steps are implemented, the mentioned use cases far exceed the typical onboard monitoring applications foreseen for conventional black-box digital twins, discussed in the introduction. Such a new physics-based (engine) digital twin with its enhanced predictivity would enable coordinated engine-generator model-based control strategies for superior efficiency and grid response time. The above development steps are still to be followed-up with the baseline created in this research, but the developed FRM-based power plant model already can be used to design and calibrate plant controllers offline.

Note that using the engine model in the load feedback mode, as foreseen for actual control applications will also add a calculation step. However, the mechanical dynamics compared to the detailed flow, heat transfer and combustion, as targeted here, is numerically simplistic and do not pose any noticeable calculation burden. A further path towards computational efficiency improvement is embedding the computationally-demanding part of the code on a Field-Programmable Gate Array (FPGA). In power plant modelling, for instance, Martins *et al.* [43] developed an FPGA-based platform for rapid prototyping of digital control for power electronic converters. The authors reported the possible use of switching frequencies of up to hundreds of kHz, resulting in real-time simulation time steps of 200–300 ns – an order of magnitude smaller compared to the ones achieved for the electrical system in this work.

5. Conclusions

The present work for the first time aims to include a fully physics-based combustion engine model in a complete power plant digital twin implementation. The conclusions below give an account to what extent this objective has been met.

- An engine model capable of real-time simulation can be developed directly from the detailed one-dimensional engine model without making cardinal simplifications to the governing physics. The lumped volume fast-running model (FRM) was accurate to within 5% of the real engine in cardinal performance parameters, and had a real-time factor of 0.35 on a standard desktop computer.
- The electrical component model, consisting of generator, FC, battery energy storage system and necessary controllers is a mix of dynamic and average-value submodels. It exerts stand-alone accuracy within the generator circuit measurement errors, maintaining real-time task execution times of 7.6 μs on average.
- The accuracy of the coupled engine-electric model in desktop co-simulation is roughly 2% worse in terms of governing electrical signals, compared to generator-to-grid simulation with imposed active power reference. This is considered sufficiently accurate for control and monitoring applications, given that the trends are predicted very well.
- The electric model does not pose any real-time restrictions and is runnable with 50 μs integration time-step size, even on a legacy real-time target computer. Implementation of the engine model on the same target computer was limited to 1 s integration time-step to prevent overruns.
- The above shortcoming, partially solvable by moving to a state-of-the-art target computer, impacts the detail crank-angle based insight into in-cylinder pressure and temperature on a real-time basis, but all mean-value derivatives are represented correctly.
- Task execution times of 0.81 s, although suitable for own real-time engine control applications, hinders real-time target implementation of the engine FRM in a full power plant model. Incremental simplification of the present FRM by using a mean-value combustion model is necessary for moving towards a full physics-based power plant digital twin. Such development, although limited in advanced combustion-control features, will offer real-time functionalities far beyond the current state of the art in power plant digital twins.

CRediT authorship contribution statement

Emma Söderäng: Conceptualization, Methodology, Formal analysis, Investigation, Visualization, Data curation, Writing – original draft, Writing – review & editing. **Saana Hautala:** Methodology, Formal analysis, Writing – review & editing. **Maciej Mikulski:** Conceptualization, Investigation, Funding acquisition, Project administration, Supervision, Writing – original draft, Writing – review & editing. **Xiaoguo Storm:** Investigation, Writing – original draft. **Seppo Niemi:** Funding acquisition, Project administration, Supervision, Resources, Writing – review & editing.

Declaration of Competing Interest

The authors declare that they have no known competing financial interests or personal relationships that could have appeared to influence the work reported in this paper.

Acknowledgement

This research was funded by Business Finland partly under the project ‘Integrated Energy Solutions to Smart and Green Shipping’ (7889/31/2017) and partly under the project ‘Clean Propulsion Technologies’ (38485/31/2020).

References

[1] “The Paris Agreement | UNFCCC.” https://unfccc.int/process-and-meetings/the-paris-agreement/the-paris-agreement (accessed Jun. 04, 2021).
[2] “What is the Kyoto Protocol? | UNFCCC.” https://unfccc.int/kyoto_protocol (accessed Sep. 21, 2021).
[3] “The European Green Deal.” Accessed: Jun. 04, 2021. [Online]. Available: https://ec.europa.eu/info/sites/default/files/european-green-deal-communication_en.pdf.
[4] European Commission, “EU Emissions Trading System (EU ETS),” *Climate Action - European Commission*, Nov. 23, 2016. https://ec.europa.eu/clima/policies/ets_en (accessed Jun. 07, 2021).
[5] “Engine Power Plants.” https://www.eugine.eu/engine-power-plants/facts-and-figures/index.html (accessed Jun. 07, 2021).
[6] Ritari A, Huotari J, Halme J, Tammi K. Hybrid electric topology for short sea ships with high auxiliary power availability requirement. Energy 2020;190:1–12. https://doi.org/10.1016/j.energy.2019.116359.
[7] International Maritime Organization (IMO), “Energy Efficiency Measures.” https://www.imo.org/en/OurWork/Environment/Pages/Technical-and-Operational-Measures.aspx (accessed Jun. 07, 2021).

[8] Skjong E, Volden R, Rodskar E, Molinas M, Johansen TA, Cunningham J. Past, present, and future challenges of the marine vessel's electrical power system. IEEE Trans Transp Electrification 2016;2(4):522–37. https://doi.org/10.1109/TTE.2016.2552720.

[9] Lopes JAP, Madureira AG, Matos M, Bessa RJ, Monteiro V, Afonso JL, et al. The future of power systems: challenges, trends, and upcoming paradigms. WIREs Energy Environ 2020;9(3). https://doi.org/10.1002/wene.368.

[10] Mikulski M, Balakrishnan PR, Doosje E, Bekdemir C. Variable Valve Actuation Strategies for Better Efficiency Load Range and Thermal Management in an RCCI Engine, 2018: 2018-01–0254. doi: 10.4271/2018-01-0254.

[11] Qian Y, Zhang Z, Deng K. Development of a three-phase sequential turbocharging system with two unequal-size turbochargers. Int J Rotating Mach 2012;2012:1–8. https://doi.org/10.1155/2012/951096.

[12] McTaggart-Cowan G, Mann K, Huang J, Singh A, Patychuk B, Zheng ZX, et al. Direct injection of natural gas at up to 600 bar in a pilot-ignited heavy-duty engine. SAE Int J Engines 2015;8(3):981–96.

[13] Raut A, Bidarvatan M, Borhan H, Shahbakhti M. Model Predictive Control of an RCCI Engine, in *2018 Annual American Control Conference (ACC)*, Milwaukee, WI, 2018, pp. 1604–1609. doi: 10.23919/ACC.2018.8431172.

[14] Mikulski M, Ramesh S, Bekdemir C. Reactivity controlled compression ignition for clean and efficient ship propulsion. Energy 2019;182:1173–92. https://doi.org/10.1016/j.energy.2019.06.091.

[15] Jaurola M, Hedin A, Tikkanen S, Huhtala K. Optimising design and power management in energy-efficient marine vessel power systems: a literature review. J Mar Eng Technol 2019;18(2):92–101. https://doi.org/10.1080/20464177.2018.1505584.

[16] Geertsma RD, Negenborn RR, Visser K, Hopman JJ. Design and control of hybrid power and propulsion systems for smart ships: a review of developments. Appl Energy 2017;194:30–54. https://doi.org/10.1016/j.apenergy.2017.02.060.

[17] Ghimire P, Park D, Zadeh MK, Thorstensen J, Pedersen E. Shipboard electric power conversion: system architecture, applications, control, and challenges [Technology Leaders]. IEEE Electrification Mag 2019;7(4):6–20. https://doi.org/10.1109/MELE.2019.2943948.

[18] Manngård M, Lund W, Björkqvist J. "Using Digital Twin Technology to Ensure Data Quality in Transport Systems," in *Proceedings of TRA2020, the 8th Transport Research Arena: Rethinking transport – towards clean and inclusive mobility*, Mar. 2020, pp. 1–8. [Online]. Available: https://www.researchgate.net/publication/339875335_Using_Digital_Twin_Technology_to_Ensure_Data_Quality_in_Transport_Systems.

[19] Perabo F, Park D, Zadeh MK, Smogeli O, Jamt L. Digital Twin Modelling of Ship Power and Propulsion Systems: Application of the Open Simulation Platform (OSP), in *2020 IEEE 29th International Symposium on Industrial Electronics (ISIE)*, Delft, Netherlands, Jun. 2020, pp. 1265–1270. doi: 10.1109/ISIE45063.2020.9152218.

[20] Bondarenko O, Fukuda T. Development of a diesel engine's digital twin for predicting propulsion system dynamics. *Energy* 2020; 196 (Special issue dedicated to 2nd International Conference on Modelling and Optimisation of Ship Energy Systems (MOSES2019)): 117–26, doi: 10.1016/j.energy.2020.117126.

[21] Urazayev D, Bragin D, Zykov D, Hafizov R, Pospelova I, Shelupanov A. Distributed Energy Management System with the Use of Digital Twin, in *2019 International Multi-Conference on Engineering, Computer and Information Sciences (SIBIRCON)*, Novosibirsk, Russia, Oct. 2019, pp. 0685–0689. doi: 10.1109/SIBIRCON48586.2019.8958118.

[22] Park H-A, Byeon G, Son W, Jo H-C, Kim J, Kim S. Digital twin for operation of microgrid: optimal scheduling in virtual space of digital twin. Energies Oct. 2020; 13(20):1–15. https://doi.org/10.3390/en13205504.

[23] He X, Ai Q, Qiu RC, Zhang D, Preliminary Exploration on Digital Twin for Power Systems: Challenges, Framework, and Applications, *ArXiv190906977 Eess Stat*, pp. 1–8, Sep. 2019.

[24] Vasudev A, Mikulski M, Balakrishnan PR, Storm X, Hunicz J. Thermo-kinetic multi-zone modelling of low-temperature combustion engines: A comprehensive review. Prog Energy Combust Sci 2022;91:100998.

[25] Wärtsilä Finland Oy, "Wärtsilä 20 Product Guide," 2020. https://cdn.wartsila.com/docs/default-source/product-files/engines/ms-engine/product-guide-o-e-w20.pdf?sfvrsn=6.

[26] Hautala S, Mikulski M, Söderäng E, Storm X, Niemi S. Towards a digital-twin of a mid-speed marine engine: from detailed 1D engine model to real-time implementation on a target platform. Int J Engine Res 2022 (In press).

[27] Domínguez-García JL, Gomis-Bellmunt O, Trilla-Romero L, Junyent-Ferré A. Indirect vector control of a squirrel cage induction generator wind turbine. Comput Math Appl 2012;64(2):102–14. https://doi.org/10.1016/j.camwa.2012.01.021.

[28] Hernandez Navas MA, Azcue Puma JL, Sguarezi Filho AJ. Direct torque control for squirrel cage induction generator based on wind energy conversion system with battery energy storage system, in *2015 IEEE Workshop on Power Electronics and Power Quality Applications (PEPQA)*, Bogota, Colombia, Jun. 2015, pp. 1–6. doi: 10.1109/PEPQA.2015.7168203.

[29] Simulink - MathWorks Nordic, "Model dynamics of three-phase asynchronous machine, also known as induction machine, in SI or pu units." https://se.mathworks.com/help/physmod/sps/powersys/ref/asynchronousmachine.html (accessed Jun. 07, 2021).

[30] MATLAB & Simulink - MathWorks Nordic, "Wind Farm - Synchronous Generator and Full Scale Converter (Type 4) Average Model." https://se.mathworks.com/help/physmod/sps/ug/wind-farm-synchronous-generator-and-full-scale-converter-type-4-average-model.html (accessed Jun. 07, 2021).

[31] F. Díaz-González, A. Sumper, and O. Gomis-Bellmunt, *Energy Storage in Power Systems*. New York, UNITED KINGDOM: John Wiley & Sons, Incorporated, 2016. Accessed: Jun. 07, 2021. [Online]. Available: http://ebookcentral.proquest.com/lib/tritonia-ebooks/detail.action?docID=4443208.

[32] Bouaziz B, Faouzi B, Gasmi M. Wind energy conversion system with full-scale power converter and squirrel cage induction generator. Int J Phys Sci 2012;7(46):6093–104. https://doi.org/10.5897/IJPS12.406.

[33] Simulink - MathWorks Nordic, "Generic battery model." https://se.mathworks.com/help/physmod/sps/powersys/ref/battery.html (accessed Jun. 04, 2021).

[34] Miao Z, Xu L, Disfani VR, Fan L. An SOC-based battery management system for microgrids. IEEE Trans Smart Grid 2014;5(2):966–73. https://doi.org/10.1109/TSG.2013.2279638.

[35] Isermann R, editor. Engine Modeling and Control. Berlin, Heidelberg: Springer Berlin Heidelberg; 2014.

[36] Gamma Technologies LLC, "GT-Suite Engine Performance Application Manual." Gamma Technologies, 2020.

[37] ABB, "615 series 5.0 FP1 IEC, Technical Manual," 2018. https://search.abb.com/library/Download.aspx?DocumentID=1MRS756887&LanguageCode=en&DocumentPartId=&Action=Launch (accessed Jun. 11, 2021).

[38] Schneider Electric, "VAMP 260 Power monitoring unit, user manual," 2015. https://download.schneider-electric.com/files?p_enDocType=User+guide&p_File_Name=V260_EN_M_B012.pdf&p_Doc_Ref=V260_EN_M_B012 (accessed Jun. 14, 2021).

[39] Kline S, McClintock F. Describing uncertainties in single-sample experiments. Mech Eng 1953;75:3–8.

[40] Speedgoat, "Speedgoat -Simulink Real-time Workflow." https://www.speedgoat.com/learn-support/simulink-real-time-workflow (accessed Jun. 04, 2021).

[41] Courant R, Friedrichs K, Lewy H. On the partial difference equations of mathematical physics. IBM J Res Dev 1967;11(2):215–34. https://doi.org/10.1147/rd.112.0215.

[42] MATLAB & Simulink - MathWorks Nordic, "Real-Time Model Preparation Workflow - MATLAB & Simulink." https://se.mathworks.com/help/physmod/simscape/ug/real-time-model-preparation-workflow.html (accessed Jun. 04, 2021).

[43] Martins J, *et al.*, Test Platform for Rapid Prototyping of Digital Control for Power Electronic Converters, in *IECON 2019 - 45th Annual Conference of the IEEE Industrial Electronics Society*, Lisbon, Portugal, Oct. 2019, pp. 2056–2061. doi: 10.1109/IECON.2019.8927836.